Tnfaip3/A20 deficient dendritic cells induce autoimmune pathology in mice, independent of T-B cell communication.

Tridib Das, Ingrid M. Bergen, Anne Huber, Menno van Nimwegen, Jennifer van Hulst, Geert van Loo, Bart N. Lambrecht, Mirjam Kool, Rudi W. Hendriks

Manuscript in preparation

ABSTRACT

Dendritic cells (DCs) are sentinel cells regulating both immune homeostasis and immunogenic responses. Ablation of *Tnfaip3*/A20, a negative regulator of the NF-κB pathway, in DCs (*Tnfaip3*$^{CD11c\text{-}KO}$ mice) induces DC activation. As a result, activation of T cells and B cells occurs leading to spontaneous germinal center (GC) formation and an autoimmune phenotype. *In vitro Tnfaip3*-deficient DCs are potent activators of naïve B cells that develop into IgG1- and IgA-producing plasma cells. We hypothesize that T cells might be dispensable for B cell-driven autoimmunity in *Tnfaip3*$^{CD11c\text{-}KO}$ mice.

Tnfaip3^{CD11c} mice were crossed to *Cd40lg*^{KO} mice to hamper communication between T cells and B cells and immune activation and tissue inflammation were examined. In 10-week-old *Tnfaip3*$^{CD11c\text{-}KO}$ mice, splenic DCs harbor an activated phenotype as evidenced by higher CD40 surface expression, both on a WT and on a *Cd40lg*^{KO} background. As expected, both follicular T helper (Tfh)-cells and GC B cells were reduced in CD40L-deficient mice. Marginal zone B cells, but not follicular B cells, expressed GC-associated cytokine receptors in *Tnfaip3*$^{CD11c\text{-}KO}$*Cd40lg*^{KO} mice. In 24-week-old *Tnfaip3*$^{CD11c\text{-}KO}$ mice, splenic IgG1^{+} plasma cells and memory B cells were highly abundant, together with elevated anti-dsDNA IgG1 in serum and IgG deposition in the kidneys. Importantly, *Tnfaip3*$^{CD11c\text{-}KO}$*Cd40lg*^{KO} mice presented with kidney pathology, in which IgA was deposited and serum anti-dsDNA IgM and IgA levels were enhanced.

These findings indicate that kidney pathology can occur in the absence of CD40L-dependent communication between T cells and B cells in mice harboring *Tnfaip3*-deficient DCs. We conclude that therapies interfering with CD40-CD40L interaction may not fully prevent organ inflammation in autoimmune disorders.

INTRODUCTION

Immune homeostasis is critically controlled by dendritic cells (DCs)[1]. In order to respond to pathogens, DCs are activated and induce an appropriate immune response to clear the infection. In autoimmunity, unfortunately, DCs are activated with deleterious consequences[2]. For instance, artificial activation of DCs, by *in vivo* ablation of *Tnfaip3*/A20, a negative regulator of NF-κB signaling, resulted in T cell and B cell activation, antibody class switching, systemic inflammation and glomerulonephritis. When mice were 24 weeks old, they developed an autoimmune phenotype resembling either inflammatory bowel disease[3] or systemic lupus erythematosus (SLE)[4].

SLE is a multifactorial disease in which multiple immune cells, such as DCs, T cells and B cells play a role[5]. The presence of antinuclear antibodies (ANA) in serum is generally considered a decisive diagnostic sign of SLE. These antibodies are produced by plasma cells, which develop from B cells that are either activated in germinal centers (GC) or by extrafollicular responses in a T cell-independent (TI) manner[6]. B-cell activation is initiated by engagement of specific antigens to the B-cell receptor (BCR), resulting in a T cell dependent or TI humoral response[7]. GC B cells are dependent on T cell help, whereby CD40L expression on activated T cells and their IL-21 production is crucial for communication with B cells[8]. Within the GC, T cell help promotes immunoglobulin (Ig) class switch, especially to IgG1[9] and IgG2[10]. However, B cells can also be activated, differentiate, and isotype-switch independent of antigen-specific T cell help, CD40L signaling, and IL-21 signaling to B cells. When B cells are activated in extrafollicular responses in a TI manner, antigen presenting cells such as DCs or macrophages can replace the function of T cells to instruct plasma cell formation[11]. Nevertheless, T cells do dramatically enhance the response, and this occurs via CD40L and IL-21 signals.

Intriguingly, *Tnfaip3*-deficient bone marrow-derived DCs (BM-DCs), when cultured with naïve B cells, could induce plasma cell formation and IgG1 and IgA class switch in a TI manner[4]. This was partially dependent on the presence of IL-6, and not due to IL-21 or other familiar TI-cytokines, such as B lymphocyte stimulator protein (BLyS, also known as BAFF) or a proliferation-inducing ligand (APRIL)[4].

It is currently unknown whether B cell activation *in vivo* in autoimmune *Tnfaip3*$^{CD11c\text{-}KO}$ mice is dependent on T cell help or directly induced by activated DCs. To determine whether T cell dependent contact was necessary, we hampered T cell communication with B cells by deletion of CD40L and crossed *Tnfaip3*$^{CD11c\text{-}KO}$ mice to CD40L-deficient mice[12].

MATERIALS AND METHODS

Mice

C57BL/6 *Tnfaip3*$^{fl/fl}$*Cd11c*$^{cre/+}$ mice[4] were crossed with *Cd40lg*^{KO} mice[12] (The Jackson Laboratory, Bar Harbor, ME, USA). Male and female mice were analyzed at 10 weeks or 24 weeks of age. The cre-deficient littermates served as wild-type (WT) controls. Mice were bred and housed under specific pathogen-free conditions in the Erasmus MC experimental animal facility. All experiments were approved by the animal ethical committee of the Erasmus MC (EMC3329).

Generation of bone marrow-derived dendritic cells (BM-DCs)

To obtain BM-DCs, BM cells were cultured for 9 days in DC culture medium (RPMI 1640 containing GlutaMAX (Invitrogen, Waltham, MA, USA, with 5% FCS (Hyclone, South Logan, UT, USA), 50 µM 2-mercaptoethanol (Sigma-Aldrich Co., St. Louis, MO, USA) and 50 µg/ml gentamycin (Invitrogen), with 20 ng/ml of granulocyte-macrophage colony-stimulating factor (GM-CSF)[13].

RNA Sequencing

Total RNA was extracted from BM-DCs as described[14]. Single-end reads were aligned to the mouse genome (UCSC Genome Browser mm9) using TopHat (Tophat version 2.0.8). Gene expression levels as fragments per kilobase of a transcript per million mapped reads (FPKMs) were calculated using Cufflinks[15]. RNA-Seq Data Analysis Differential gene expression assessment was done in the R environment (version 3.1.1) with CuffDiff[16]. Gene set enrichment analysis (GSEA)[17] was performed using a pre-ranked list of all genes. The MySigDB collection "H: Hallmark Genes" was used to align for enrichment. From the top 3 most enriched gene sets results, we further specified cytokines and chemokines as published on www.genenames.org.

Tissue preparation

Spleens were taken from sacrificed mice. One half was stored in Tissue-Tek® O.C.T.™ compound (Sakura Finetek Europe B.V., Alphen aan den Rijn, The Netherlands) and slowly frozen at -20 °C. Cryo sections were cut using a CryoStar™ NX70 Cryostat (Thermo Fisher Scientific Inc., Waltham, MA, USA).

The other half was used to obtain single cell suspensions. Spleens were homogenized through a 100-µm cell strainer (Corning Inc., Corning, NY, USA) and collected in Gibco™ RPMI Medium 1640 (1 x) + GlutaMAX™-1 (Thermo Fisher Scientific Inc., Waltham, MA, USA). Spleen red blood cells were lysed using osmotic lysis buffer (0.15 M NH_4CL, 10 mM $KHCO_3$, 0.1 mM EDTA, pH 7.1-7.4; sterile-filtered with 0.22 µm filter).

Freshly isolated kidneys, liver, and pancreas were incubated 24 hrs on Roti-Histofix 4% (Carl-Roth, Karlsruhe, Germany) and then embedded in paraffin wax. Paraffin embedded tissue sections were stained with hematoxylin and eosin, using standard procedures.

Flow cytometry and cell sorting

Flow cytometric surface and intracellular staining procedures have been described previously[18]. Monoclonal antibodies used for flow cytometric analyses were (Target, Clone, Manufacturer): CD11b (M1/70, BD Biosciences), CD11c (N418, Invitrogen), CD19 (1D3, BD Biosciences), CD21 (4E3, eBioscience), CD23 (B3B4, eBioscience), CD3e (17A2, eBioscience), CD4 (GK1.5, eBioscience), CD80 (16-10A1, eBioscience), CD86 (GL1, BD Biosciences), CD95 (Jo2, BD Biosciences), CXCR5 (2G8, BD Biosciences), GL7 (RUO, BD Biosciences), IgD (11-26c.2a, BD Biosciences), IgG1 (R19-15, BD Biosciences), IgM (II/41, eBioscience), MHC-II (M5/114.15.3, eBioscience), PD-1 (J43, BD Biosciences), The following monoclonal antibodies were used for cell sorting (Target, Clone, Manufacturer): CD19 (eBio1D3, eBioscience), CD21 (4E3, eBioscience), CD23 (B3B4, eBioscience), CD3e (145-2C11, BD Biosciences). Sorting was conducted using a BD FACSAria™ II (BD Biosciences, San Jose, CA, USA). Data analysis was performed in FlowJo version 9 Workspace (FlowJO LLC, Ashland, OR, USA).

RNA isolation and cDNA synthesis

Total RNA was isolated from sorted follicular (FO) B cells and marginal zone (MZ) B cells, using the RNeasy® Micro Kit (QIAGEN, Venlo, Netherlands) according to the manufacturer's instructions. cDNA was synthesized using the RevertAid H Minus First Strand cDNA Synthesis Kit (Thermo Fisher Scientific Inc., Waltham, MA, USA). 11 µl of the isolated total RNA was used and 1 µl of random hexamer primer was added, then mixed, centrifuged and incubated for 5 min at 65 °C. The mixture was chilled on ice, centrifuged and 4 µl of 5x Reaction Buffer, 1 µl of RiboLock RNase Inhibitor (20U/µl), 2 µl 10 mM dNTP Mix and 1 µl RevertAid H Minus Reverse Transcriptase (200U/µl) were added. After incubation for 5 min at 25 °C, the mixture was incubated for 60 min at 42 °C. To terminate the reaction, the sample was heated to 70 °C for 5 min. The cDNA was stored at -20 °C until it was used in quantitative RT-PCR.

Quantitative RT-PCR

Quantitative RT-PCR (real-time reverse-transcription PCR) analysis was performed using the SYBR® Select Master Mix Kit (Thermo Fisher Scientific Inc., Waltham, MA, USA) and primers (Target, Forward, Reverse) for Fasl (F: GCAGAAGGAACTGGCAGAAC, R: TTAAATGGGCCACACTCCTC), Il-4r (F: GAGTGGAGTCCTAGCATCACG, R: CAGTGGAAGGCGCTGTATC), Il-21 (F: CCATCAAACCCTGGAAACAA, R: TCACAGGAAGGGCATTTAGC) and Il-21r (F: AGTGCCCCAGCCTAAAGAAT, R: ACTGAGTATGCTGGGGTTGG) on an Applied Biosystems™

7300 Real Time PCR System (Thermo Fisher Scientific Inc., Waltham, MA, USA). Ubiquitin C (UBC) mRNA expression was used as housekeeping gene to normalize gene transcription. Data were extracted from the linear range of amplification.

Immunoglobulin levels and autoreactivity assessment

Serum total immunoglobulin levels were assessed by ELISA, as previously described[19]. Briefly, goat-anti-mouse immunoglobulins were plated overnight. Wells were blocked and serum was incubated for 3 hrs at room temperature. Depending on the isotype of interest, anti-mouse biotin labeled against the isotype of interest was incubated and developed. The optical density (OD) was measured at 450 nm on a Microplate Reader (Bio-Rad, Hercules, CA, USA). Immunoglobulin autoreactivity assessment was assessed as previously described[19].

Periodic Acid Schiff Diastase staining (PAS-D or PAS+ staining)

Three-µm-thick paraffin embedded kidney sections were stained with Periodic Acid Schiff (PAS; Sigma-Aldrich). Briefly, paraffin embedded sections were dewaxed and hydrated to water using Xylene (Sigma-Aldrich) and ethanol dilutions in MilliQ. One part human saliva (containing the enzyme diastase) was diluted 1:10 with MilliQ and incubated on slides for 30 min on room temperature. Slides were placed for 5 min in freshly prepared periodic acid solution (Sigma-Aldrich) and then in Schiff's reagent for 5 min and counterstained with Gill's hematoxylin (Merck Millipore) for 2 sec. Lastly, slides were dehydrated using Xylene and mounted in Entallan (Merck Millipore).

Immunohistochemistry of Cryosections

For immunohistochemistry, 6 µm acetone or 4 % formalin fixed spleen sections were blocked in peroxidase blocking buffer (PBS, 0.67 % H_2O_2, 2 % NaN_3) for 30 min at room temperature. Aspecific secondary antibody binding was prevented by blocking the sections in Blocking Buffer (1% Blocking Reagent (Roche Diagnostics GmbH, Mannheim, Germany) in PBS) containing 10% normal goat or donkey serum. Sections were stained with primary antibodies for 1 hr at room temperature, washed three times with PBS and incubated with alkaline phosphatase (AP) or peroxidase (PO) conjugated secondary antibodies for 30 min at room temperature. Used antibodies are listed (Target, clone, dilution, manufacturer, secondary antibody, dilution, manufacturer): CD21 (Biotin, 1:100, Streptavidin PO, 1:50), MOMA1 (1:100, Bioceros, Goat anti-Rat AP, 1:50, Jackson Immunoresearch), GL7 (RUO, 1:50, eBioscience, Goat anti-Rat AP, 1:50, Jackson Immunoresearch) and IgD (11-26, 1:50, eBioscience, Goat anti-PE PO, 1:50, Rockland Immunochemichals). First the alkaline phosphatase was detected in 30 minutes using a mixture containing N-(4-Amino-2,5-diethoxyphenyl)benzamide (Fast Blue BB, Sigma-Aldrich), 2 M HCl, 4 % $NaNO_2$, Naphthol AS-MX phosphate (VWR International, Radnor,

PA, USA), N,N-dimethylformamide (DMF) (Sigma-Aldrich), Tris-HCl buffer (pH 8.5) and (-)-tetramisole hydrochloride (Sigma-Aldrich). The substrate was filtered using filtration paper. Subsequently, peroxidase was detected within 30 min with a mixture containing 3-amino-9-ethylcarbazole (AEC) in DMF, 0.1 M NaAC (pH 4.6), 30% H_2O_2 (Merck Millipore, Darmstadt and double-filtered. Stained tissue sections were embedded in Kaiser's Glycerol/Gelatin (Boom B.V., Meppel, The Netherlands). Micrographs were made using a Leica DM2000 microscope (Leica Microsystems GmbH, Wetzlar, Germany), a Leica DFC450 camera (Leica Microsystems GmbH, Wetzlar, Germany) and Leica Application (LAS) Software Version 4.5.0 (Leica Microsystems GmbH, Wetzlar, Germany).

Immunohistochemistry of Paraffin embedded sections

For immunohistochemical stainings on paraffin embedded sections, antigen retrieval was established using citrate buffer (Sigma Aldrich) pH 6.0 for 10 min in the microwave. 3 µm-thick paraffin kidney sections were stained with biotinylated primary antibody against total Immunoglobulin Isotypes (Primary antibody target, dilution, manufacturer): IgA (Biotin, 1:200, Southern Biotech), IgM (Biotin, 1:200, Southern Biotech) and IgG (Biotin, 1:200, Southern Biotech). After washing with PBS, slides were incubated for 1 hr with Avidin/Biotinylated Enzyme Complex (ABC) from the anti-Rat ABC Peroxidase Kit (Vector Laboratories). 10mg 3,3'-Diaminobenzene (DAB) (Sigma-Aldrich) was dissolved in Tris-HCl buffer (pH 7,6) with 12µl H_2O_2 to retrieve specific staining and slides were coated with Kaiser's glycerol.

Confocal Microscopy

For confocal imaging, 12 µm-thick spleen cryostat sections were stained as explained above. Primary and secondary antibodies were (Target, clone, dilution, manufacturer, with respective secondary antibody target, dilution, manufacturer): B220 (RA3-6B2, 1:50, BD Biosciences, Donkey anti-Rat Cy5, 1:200, Jackson Immunoresearch), CD11c (N418, 1:10, eBioscience, Goat anti-Hamster Cy3, 1:1000, Jackson Immunoresearch), CD3e (KT3, 1:50, Bioceros, Donkey anti-Rat Cy3, 1:1000, Jackson Immunoresearch). Slides were counterstained with *4',6-diamidino-2-phenylindole (*DAPI), mounted with VECTASHIELD® HardSet™ Antifade Mounting Medium (Vector Laboratries, Burlingame, CA, USA) and analyzed on a Zeiss LSM 510 META confocal microscope (Carl Zeiss AG, Oberkochen, Germany). Images were analyzed using ImageJ software (Rasband, W.S., ImageJ, U. S. National Institutes of Health, Bethesda, Maryland, USA).

Statistics

Statistical significance of data was calculated using the non-parametric Mann-Whitney U test. P-values <0.05 were considered significant. All analyses were performed using Prism (GraphPad Software version 9, La Jolla, CA, USA). All data are presented as the mean with the standard error of the mean (SEM).

RESULTS

Loss of *Tnfaip3*/A20 in BM-DCs increases the expression of cytokines involved in B cell activation.

As *in vitro Tnfaip3*/A20-deficient BM-DCs can directly activate B cells[4], an unbiased transcriptome analysis using mRNA-sequencing was performed[14] to examine differences between *Tnfaip3*^{WT}, *Tnfaip3*^{HZ}, and *Tnfaip3*^{KO} BM-DCs that could explain the TI B cell activating capacity. A large number of differentially expressed genes (DEG) were identified between *Tnfaip3*^{WT}, *Tnfaip3*^{HZ}, and *Tnfaip3*^{KO} BM-DCs (**Figure 1A**). Gene set enrichment analysis (GSEA) revealed that several cytokine-signaling pathways are highly active in *Tnfaip3*^{KO} BM-DCs, with the 'TNF-α signaling via NF-κB' pathway as the most enriched gene set in *Tnfaip3*^{KO} BM-DCs compared to *Tnfaip3*^{WT} BM-DCs (**Figure 1B/C**). This pathway was also significantly enriched in *Tnfaip3*^{KO} BM-DCs when compared to *Tnfaip3*^{HZ} BM-DCs as well as in *Tnfaip3*^{HZ} BM-DCs compared to *Tnfaip3*^{WT} BM-DCs (**Supplementary Figure 1A/B**). mRNA expression of several cytokines and chemokines was increased in *Tnfaip3*^{KO} BM-DCs compared to *Tnfaip3*^{WT} BM-DCs (**Figure 1D**), including cytokines involved in activation of B cells and T cells, such as *Il6*, *Il1b*, and *Il1a* (**Figure 1E**). However, mRNA expression of some cytokines, including *Tnf* and *Lta* was reduced in *Tnfaip3*^{KO} BM-DCs compared to *Tnfaip3*^{WT} BM-DCs (**Figure 1F**). Expression of TI cytokines regulating B cell activation and survival, such as APRIL, BAFF and TGFβ were not significantly altered in *Tnfaip3*^{KO} BM-DCs (data not shown).

Taken together, cytokine signaling pathways were highly dependent on the expression of *Tnfaip3* in BM-DCs and these pathways were inversely correlated with *Tnfaip3* gene expression. *Tnfaip3*-deficient DCs harbored elevated mRNA expression of cytokines, such as IL-6, IL-1β and IL-1α that may directly influence B cell activation, particularly in the context of autoimmunity[20, 21].

Splenic DCs from *Tnfaip3*$^{CD11c\text{-}KO}$*Cd40lg*^{KO} mice show enhanced expression of activation markers.

To test whether T cell help is needed for B cell activation in *Tnfaip3*$^{CD11c\text{-}KO}$ mice, CD40L-CD40 interaction between T cells and B cells was abrogated by crossing *Tnfaip3*$^{CD11c\text{-}KO}$ mice with *Cd40lg*^{KO} mice. Spleens of 10-week-old *Tnfaip3*$^{CD11c\text{-}KO}$ mice and *Tnfaip3*$^{CD11c\text{-}KO}$*Cd40lg*^{KO} mice showed splenomegaly in comparison to their respective WT controls and *Tnfaip3*$^{CD11c\text{-}Hz}$ mice (**Supplementary Figure 1C**). However, no differences in splenic cellularity (**Supplementary Figure 1D**) was seen, consistent with the previously demonstrated extramedullary hematopoiesis in *Tnfaip3*$^{CD11c\text{-}KO}$ mice[4]. Also, the number of splenic DCs (**Supplementary Figure 1E/F**) did not differ across the six genotypes. Splenic DCs of *Tnfaip3*$^{CD11c\text{-}HZ}$ and *Tnfaip3*$^{CD11c\text{-}KO}$ mice showed a slight increase of CD40 expression, which reached significance for *Tnfaip3*$^{CD11c\text{-}HZ}$ mice, compared to WT mice

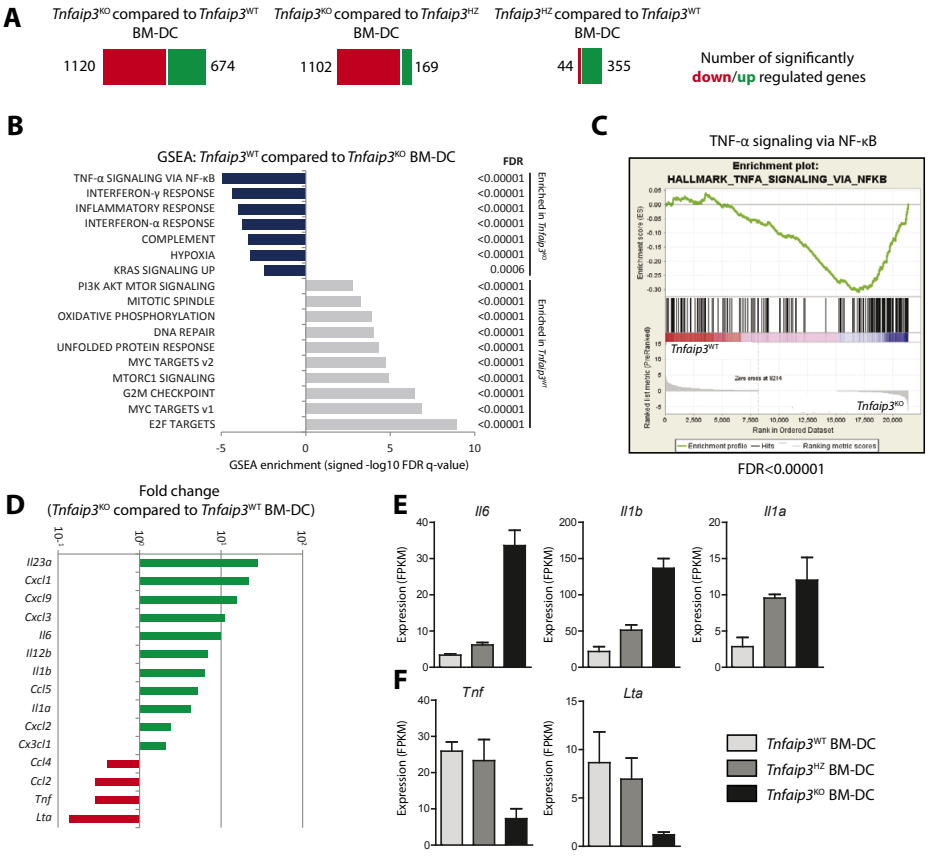

Figure 1: Loss of *Tnfaip3*/A20 in BM-DCs increases the expression of cytokines involved in B cell activation.

Bone marrow-derived DCs (BM-DCs) were analyzed by RNA Next generation sequencing (NGS). (**A**) The significant up and down-regulated gene numbers are listed according to Cuff diff-tools between *Tnfaip3*^{WT} mice, *Tnfaip3*^{HZ} mice and *Tnfaip3*^{KO} BM-DCs. (**B**) Gene set enrichment analysis (GSEA) performed for the ranked list of significantly altered genes between BM-DCs from *Tnfaip3*$^{CD11c\text{-}KO}$ mice and *Tnfaip3*$^{CD11c\text{-}WT}$ mice. The top 10 results with a False Discovery Rate (FDR)<0.25 are shown. (**C**) The top result of the GSEA with 'signal to noise'. (**D**) Using the three most enriched results (being "TNF-α SIGNALING VIA NF-κB", "INTERFERON-γ RESPONSE" and "INFLAMMATORY RESPONSE"), we characterized all cytokines and chemokines and expressed the fold changes between *Tnfaip3*^{KO} BM-DCs and *Tnfaip3*^{WT} BM-DCs. (**E-F**) Quantification of the Fragments Per Kilobase of transcript per Million mapped reads (FPKM) values of IL-6 (*Il6*), IL-1β (*Il1b*) and IL-1α (*Il1a*) (**E**) and TNF-α (*Tnfa*) and TNF-β (*Lta*) (**F**) between all BM-DC genotypes, as assessed directly from raw sequence data. NGS results are presented as mean values ± SEM of $n = 4$ mice per group.

(**Figure 2A/B**). The expression of PD-L1, but not CD86, was moderately enhanced on DCs from *Tnfaip3*$^{CD11c\text{-}KO}$ mice compared to WT controls (**Figure 2A/B**). Remarkably, in the absence of CD40L, expression of CD40, CD86, and PD-L1 were significantly increased on DCs from *Tnfaip3*$^{CD11c\text{-}KO}$*Cd40lg*^{KO} mice, compared to *Cd40lg*^{KO} mice (**Figure 2A/B**).

In short, in splenic DCs of *Tnfaip3*$^{CD11c\text{-}KO}$ mice, CD40L signals appear to restrain the expression of co-stimulatory molecules such as CD40, CD86, and PD-L1.

Reduction of MZ B cells in *Tnfaip3*$^{CD11c\text{-}KO}$ mice is restored by *Cd40lg* deletion.

In *Tnfaip3*$^{CD11c\text{-}KO}$ mice the numbers of CD4$^+$ T cells and CD8$^+$ T cells were not significantly affected (**Figure 3A**). However, the absence of CD40L signals is known to influence T cell and B cell homeostasis[22]. Both splenic CD8$^+$ and CD4$^+$ T cell numbers were reduced in 10-week-old *Cd40lg*^{KO} mice compared to WT mice (**Figure 3A**, see for gating strategy: **Supplementary Figure 2A**). Within the GC, follicular T-helper cells (Tfh-cells) are crucial for B cell activation and plasma cell formation, partly through CD40L-CD40 interaction[23]. The proportions of Tfh cells from total CD4$^+$ T cells were reduced in spleens of *Cd40lg*^{KO} mice compared to WT mice (**Figure 3B**, see for gating strategy: **Supplementary Figure 2A**). The numbers of B cells were significantly decreased in *Tnfaip3*$^{CD11c\text{-}KO}$ mice as well as in *Cd40lg*^{KO} mice compared to WT mice (**Figure 3C**, see for gating strategy: **Supplementary Figure 2B**). The proportions of GC B cells were increased in *Tnfaip3*$^{CD11c\text{-}KO}$ mice compared to WT controls and *Tnfaip3*$^{CD11c\text{-}HZ}$ mice, but these were virtually absent in mice lacking *Cd40lg* (**Figure 3C**). Despite the lack of GC B cells in all three *Tnfaip3* genotypes on the *CD40lg*^{KO} background, substantial number of plasma cells were present (**Figure 3C**, see for gating strategy: **Supplementary Figure 2B**).

Whereas the absence of the *Tnfaip3* gene in DCs did not significantly affect the proportions of follicular (FO) B cells in the spleen, marginal zone (MZ) B cell frequencies were dramatically reduced in *Tnfaip3*$^{CD11c\text{-}KO}$ mice compared to WT or *Tnfaip3*$^{CD11c\text{-}HZ}$ mice (**Figure 3D/E**). The percentages of FO B cells were slightly reduced in *Cd40lg*^{KO} mice compared to WT controls and likewise in *Tnfaip3*$^{CD11c\text{-}KO}$*Cd40lg*^{KO} mice compared to *Tnfaip3*$^{CD11c\text{-}KO}$ mice (**Figure 3E**). Intriguingly, the proportions of MZ B cells were increased in *Tnfaip3*$^{CD11c\text{-}KO}$*Cd40lg*^{KO} mice compared to *Tnfaip3*$^{CD11c\text{-}KO}$ mice, to similar frequencies as observed in WT mice (**Figure 3E**).

Next, we used immunohistochemistry to examine the splenic architecture. In WT mice rings of MOMA1$^+$ MZ macrophages were bordered by CD21$^+$ FO B cells and MZ B cells on the inside and outside, respectively (**Figure 3F**). Similar staining patterns were observed in spleens of *Cd40lg*^{KO} mice. However, the architecture was completed distorted in *Tnfaip3*$^{CD11c\text{-}KO}$ mice, as previously described[4] (**Figure 3F**), with only very few B cells and MZ macrophages. Strikingly, white pulp regions containing MZ macrophages, FO and MZ B cells were slightly reestablished in *Tnfaip3*$^{CD11c\text{-}KO}$*Cd40lg*^{KO} mice, compared to *Tnfaip3*$^{CD11c\text{-}KO}$ mice, although these regions were still smaller than those in *Cd40lg*^{KO} or WT mice (**Figure 3F**). In 24-week-old mice, the marked reduction in FO and MZ B cell was still apparent in *Tnfaip3*$^{CD11c\text{-}KO}$ mice, but less so in *Tnfaip3*$^{CD11c\text{-}KO}$*Cd40lg*^{KO} mice (**Supplementary Figure 2C**).

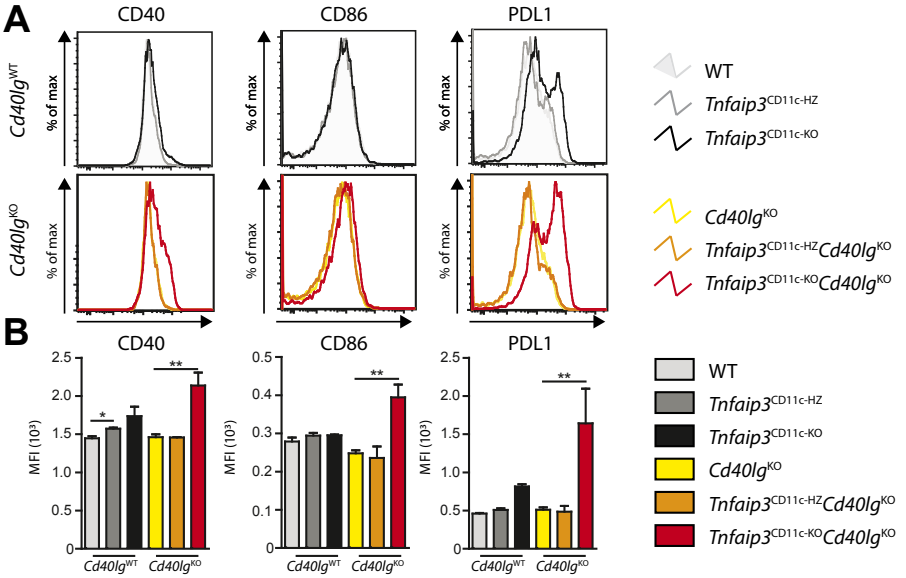

Figure 2: Splenic DCs from *Tnfaip3*$^{CD11c\text{-}KO}$*Cd40lg*^{KO} mice show enhanced expression of activation markers.

Spleens of naïve 10-week-old *Tnfaip3*^{CD11c}*Cd40lg* mice were analyzed for DCs (CD11c^{+}MHC-II^{+}) (**A-B**) Quantification of DC activation for CD40, CD86 and PD-L1 histograms (**A**) and bar-plot (**B**) using flow cytometry. Results are presented as mean values ± SEM of *n* = 2-5 mice per group. **P<0.01.

Taken together, in the absence of CD40L expression, mice harboring *Tnfaip3*-deficient DCs have strongly reduced Tfh-cell and GC B cell numbers. While young *Tnfaip3*$^{CD11c\text{-}KO}$ mice have very low MZ B cell proportions, these are considerably restored in the absence of CD40L, particularly in aging mice.

B cells from *Tnfaip3*$^{CD11c\text{-}KO}$*Cd40lg*^{KO} mice have an activated phenotype and T cells show robust expression of B cell-activating cytokines.

We next examined the phenotype of FO and MZ B cells. Whereas deletion of *Tnfaip3* did not affect their phenotype, we found that both FO and MZ B cells from 10-week-old *Tnfaip3*$^{CD11c\text{-}KO}$*Cd40lg*^{KO} mice displayed enhanced surface expression of CD80, CD86 and PD-L2 compared to *Cd40lg*^{KO} mice (**Figure 4A**). While both FO B cells and MZ B cell expressed enhanced CD95 in *Tnfaip3*$^{CD11c\text{-}KO}$*Cd40lg*^{KO} mice compared to *Cd40lg*^{KO} mice, only MZ B cells displayed enhanced MHC-II expression, which however did not reach significance (**Supplementary Figure 3A**).

Since interleukin IL-21 and IL-4 direct GC B cell responses[24], the expression of the IL-21 receptor (IL-21R) and IL-4R was examined in purified splenic FO and MZ B cell fractions by RT-PCR (See for sorting strategy: **Supplementary Figure 3B**). Whereas no differences were detected for IL-21R and IL-4R mRNA expression in FO B cells, minor increases were

observed in splenic MZ B cells from *Tnfaip3*$^{CD11c\text{-}KO}$*Cd40lg*^{KO} mice compared to *Cd40lg*^{KO} mice (**Supplementary Figure 3C**).

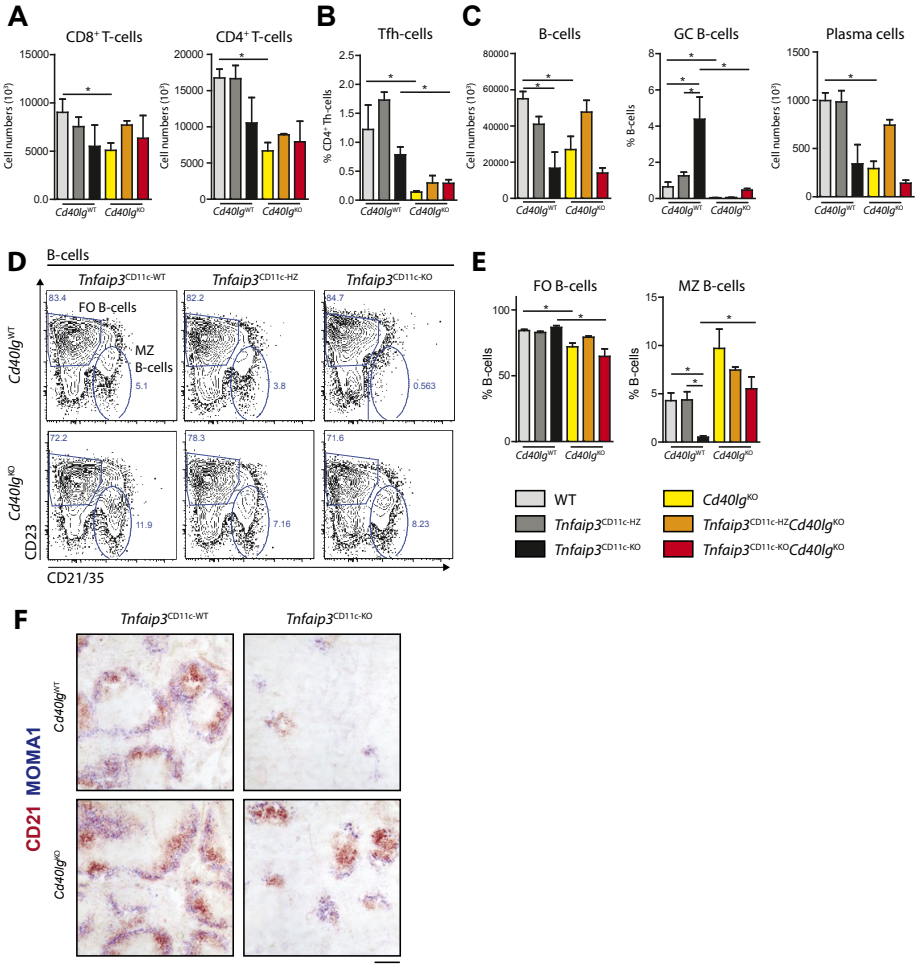

Figure 3: Reduction of MZ B cells in *Tnfaip3*$^{CD11c\text{-}KO}$ mice is restored by *Cd40lg* deletion.
Naïve 10-week-old *Tnfaip3*^{CD11c}*Cd40lg* mice spleens were analyzed for T cells and B cells. (**A-E**) Quantification of splenic CD8$^+$ T cells (CD3$^+$CD8$^+$CD4$^-$), CD4$^+$ T cells (CD3$^+$CD4$^+$CD8$^-$) (**A**), Follicular T-helper cells (Tfh-cells; CD3$^+$CD4$^+$CXCR5$^+$PD1^{hi}) (**B**), B cells (B220$^+$), Germinal center B cells (B220$^+$CD138$^-$CD95$^+$IgD$^-$), Plasma cells (B220$^-$CD138$^+$) (**C**) using flow cytometry. (**D**) Flow cytometric analysis of Follicular B cells (FO B cells; B220$^+$CD23$^+$, CD21/35^{int}) and Marginal zone B cells (MZ B cells; B220$^+$CD23$^-$, CD21/35$^+$) (**E**) Quantification of splenic FO B cell and MZ B cell proportions using flow cytometry. (**F**) Immunohistochemistry of spleens for MOMA1$^+$ (Blue) macrophages and CD21$^+$ (red) MZ B cells. Scale bars represent 200µm. Representative data is shown from one out of two independent experiments. Results are presented as mean values ± SEM of *n* = 2-5 mice per group. *P<0.05, **P<0.01.

We next investigated cytokine expression in splenic T cells. IL-21 mRNA expression in $CD3^+CD4^+CD44^+$ effector $CD4^+$ T-cells was apparently not affected by *Tnfaip3* deletion (**Figure 4B**), but was decreased in *Cd40lg*^{KO} mice and *Tnfaip3*$^{CD11c\text{-}HZ}$*Cd40lg*^{KO} mice compared to their *Cd40lg*^{WT} counterparts (**Figure 4B**). Interestingly, IL-21 mRNA expression in effector $CD4^+$ T-cells appeared to be rescued in *Tnfaip3*$^{CD11c\text{-}KO}$*Cd40lg*^{KO} mice compared to *Cd40lg*^{KO} mice (**Figure 4B**). The splenic total $CD4^+$ T cell population from *Tnfaip3*$^{CD11c\text{-}KO}$ mice contained elevated proportions of IL-4^+ cells compared to *Tnfaip3*$^{CD11c\text{-}HZ}$ mice and WT mice, as determined by intracellular flow cytometry (**Figure 4C**). Likewise, the proportions of IL-4^+ $CD4^+$ T cells from *Tnfaip3*$^{CD11c\text{-}KO}$*Cd40lg*^{KO} mice were increased compared to *Cd40lg*^{KO} mice (**Figure 4C**).

Other T cell-derived cytokines such as IFNγ, IL-6 and IL-17 can also promote B cell responses[25, 26]. The proportion of IFN-γ^+ splenic $CD4^+$ T cell did not differ within the three *Tnfaip3* genotypes on the *Cd40lg*^{WT} background, but were decreased in *Cd40lg*^{KO} mice (**Figure 4C**). A minor significant increment of IFN-γ-expressing $CD4^+$ T cells was seen in the spleen of *Tnfaip3*$^{CD11c\text{-}KO}$*Cd40lg*^{KO} mice compared to *Cd40lg*^{KO} mice (**Figure 4C**). The frequency of IL-6^+ $CD4^+$ T cells within *Tnfaip3*$^{CD11c\text{-}KO}$ mice was enhanced compared to *Tnfaip3*$^{CD11c\text{-}HZ}$ mice and WT mice (**Figure 4C**).

Interestingly, the most pronounced increase in IL-6^+ $CD4^+$ T cells was observed in *Tnfaip3*$^{CD11c\text{-}KO}$*Cd40lg*^{KO} mice (**Figure 4C**). The proportions of IL-17^+ $CD4^+$ T cells were enhanced in *Tnfaip3*$^{CD11c\text{-}KO}$ mice and *Tnfaip3*$^{CD11c\text{-}KO}$*Cd40lg*^{KO} mice (**Figure 4C**). The proportions of IFN-γ^+ $CD8^+$ T cells did not significantly differ between the six genotypes (**Figure 4D**). A prominent increase in IL-6^+ $CD8^+$ T cells was seen in *Tnfaip3*$^{CD11c\text{-}KO}$*Cd40lg*^{KO} mice compared to the other five groups of mice (**Figure 4D**).

In summary, in the absence of CD40L, FO B cells and MZ B cells from *Tnfaip3*$^{CD11c\text{-}KO}$ mice show increased expression of cell surface activation markers. Although the interaction of T cells with B cells is hampered by the absence of CD40L, $CD4^+$ and $CD8^+$ T cells from *Tnfaip3*$^{CD11c\text{-}KO}$*Cd40lg*^{KO} mice still produce B cell-activating cytokines, such as IL-21, IL-4, IFN-γ, IL-17 and IL-6.

Aged *Tnfaip3*$^{CD11c\text{-}KO}$ mice do not develop GC B cell clusters in the absence of CD40L.

As previously reported[4], aged ~24-week-old *Tnfaip3*$^{CD11c\text{-}HZ}$ mice and *Tnfaip3*$^{CD11c\text{-}KO}$ mice harbor enlarged spleens in comparison to WT mice, largely due to extramedullary hematopoiesis (**Figure 5A**). Likewise, spleens of *Tnfaip3*$^{CD11c\text{-}HZ}$*Cd40lg*^{KO} mice and *Tnfaip3*$^{CD11c\text{-}KO}$*Cd40lg*^{KO} mice were enlarged compared to *Cd40lg*^{KO} mice (**Figure 5A**). Similar to young mice, spleens of aged *Tnfaip3*$^{CD11c\text{-}KO}$ mice and *Tnfaip3*$^{CD11c\text{-}KO}$*Cd40lg*^{KO} mice lacked normal lymphoid structures compared to *Tnfaip3*$^{CD11c\text{-}HZ}$ and *Tnfaip3*$^{CD11c\text{-}WT}$ mice on a WT or *Cd40lg*^{KO} background (**Figure 5B**). The total numbers of $CD4^+$ T cells were similar in spleens in all six genotypes of aged mice (**Figure 5C**). Within the splenic $CD4^+$ T

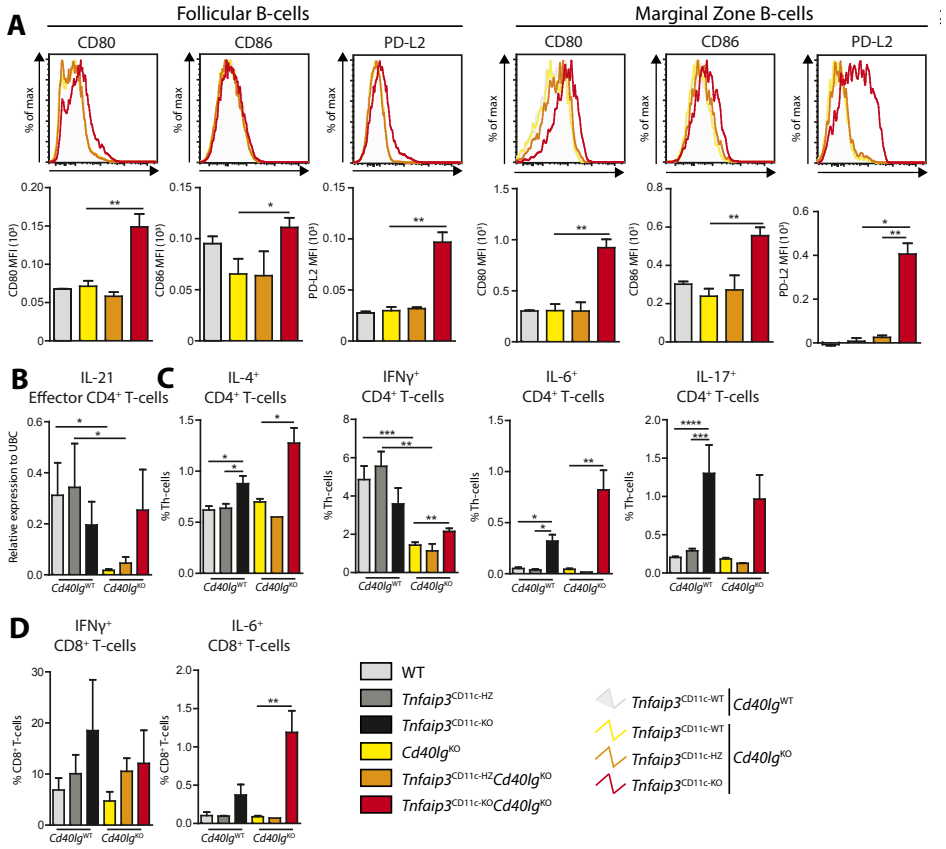

Figure 4: B cells from *Tnfaip3*$^{CD11c\text{-}KO}$*Cd40lg*^{KO} mice have an activated phenotype and T cells show robust expression of B cell-activating cytokines.

Naïve 10-week-old *Tnfaip3*^{CD11c}*Cd40lg* mice spleens were analyzed for FO B cells (CD19$^+$CD23$^+$CD21/35^{int}) and MZ B cells (CD19$^+$CD23$^-$CD21/35$^+$). Since MZ B cells were virtually absent in *Tnfaip3*$^{CD11c\text{-}KO}$ mice, only FO B cells and MZ B cells from *Tnfaip3*$^{CD11c\text{-}WT}$ mice were compared with all three *Cd40lg*^{KO} genotypes. (**A**) Histograms and bar-chart quantification of B cell activation markers CD80, CD86 and PD-L2. (**B**) Quantification of cytokines IL-21 expression in sorted effector T cells (CD3$^+$CD4$^+$CD44$^+$) using RT-PCR. (**C**) Enumeration of the proportions of intracellular IL-4$^+$, IFN-γ$^+$, IL-6$^+$ and IL-17$^+$ splenic CD4$^+$ T cells using flow cytometry. (**D**) Quantification of the proportions intracellular IFN-γ$^+$ and IL-6$^+$ CD8$^+$ T cells using flow cytometry. Data is shown from one experiment in (**A**-**B**) and pooled data from two experiments (**C**-**D**). Results are presented as mean values ± SEM of *n* = 2-7 mice per group. *P<0.05, **P<0.01, ***P<0.001, ****P<0.0001.

cells, the proportions of Tfh-cells were increased in *Tnfaip3*$^{CD11c\text{-}HZ}$ mice compared to WT mice and *Tnfaip3*$^{CD11c\text{-}KO}$ mice, but were severely reduced in the three *Tnfaip3* genotypes on the *Cd40lg*^{KO} background (**Figure 5D**). Splenic B cell numbers were reduced in aged *Tnfaip3*$^{CD11c\text{-}KO}$ mice compared to WT or *Tnfaip3*$^{CD11c\text{-}HZ}$ mice, but did not differ between the three *Tnfaip3* genotypes on the *Cd40lg*^{KO} background (**Figure 5E**). Whereas the frequencies of GC B cells were increased in spleens of *Tnfaip3*$^{CD11c\text{-}HZ}$ and *Tnfaip3*$^{CD11c\text{-}KO}$ mice, GC B

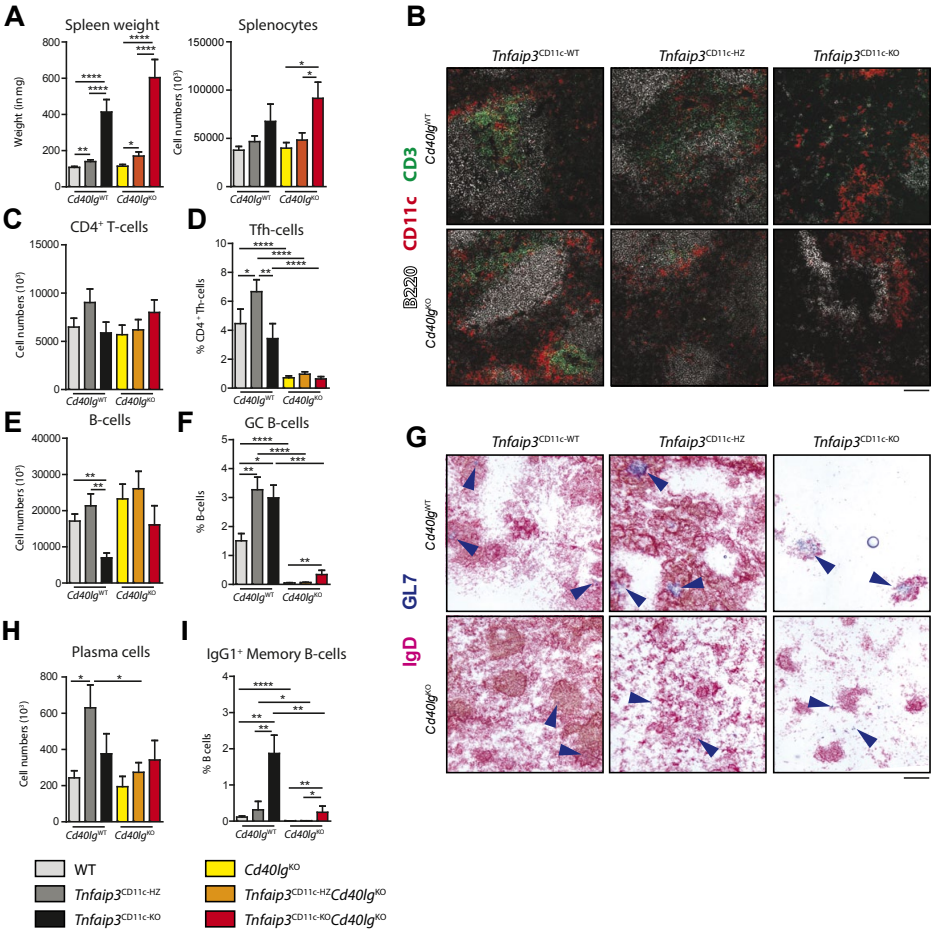

Figure 5: Aged *Tnfaip3*$^{CD11c\text{-}KO}$ mice do not develop GC B cell clusters in the absence of CD40L.
Naïve 24-week-old *Tnfaip3*^{CD11c}*Cd40lg* mice spleens were analyzed. (**A**) Enumeration of splenic weight and cellularity. (**B**) Confocal histology of spleens for CD3$^+$ (green); CD11c$^+$ (red) and B220$^+$ (white) cells. (**C-F**) Quantification of splenic CD4$^+$ T cell numbers (CD3$^+$CD4$^+$) (**C**), proportions of splenic Follicular Th-cells (Tfh-cells; CD3$^+$CD4$^+$CXCR5$^+$PD1^{hi}) (**D**), B cell (B220$^+$) numbers (**E**), and the proportions of splenic GC B cells (B220$^+$CD138$^-$CD95$^+$IgD$^-$) (**F**) using flow cytometry. (**G**) Immunohistochemistry of spleens for IgD$^+$ (Pink) and GL7$^+$ (Blue). (**H-I**) Quantification of splenic plasma cells (B220$^-$CD138$^+$) (**H**) and splenic memory IgG1$^+$ memory B cells (B220$^+$CD138$^-$IgG1$^{+(surface)}$) using flow cytometry. Results are pooled from 5-7 independent experiments and are presented as mean values ± SEM of *n* = 11-16 mice per group. Scale bars represent 200µm. *P<0.05, **P<0.01, ***P<0.001, ****P<0.0001.

cells were virtually absent in aged *Cd40lg*^{KO} and *Tnfaip3*$^{CD11c\text{-}HZ}$*Cd40lg*^{KO} mice (**Figure 5F**). Although B cells with a GC surface phenotype were detected in *Tnfaip3*$^{CD11c\text{-}KO}$*Cd40lg*^{KO} mice (**Figure 5F**), GL7$^+$ B cells were only present as isolated B cells and no GC B cell clusters could be observed (**Figure 5G**). The numbers of splenic plasma cells were elevated in old *Tnfaip3*$^{CD11c\text{-}HZ}$ mice compared to WT controls (**Figure 5H**). Comparable to

young mice, splenic plasma cell counts did not differ significantly between three *Tnfaip3* genotypes on the *Cd40lg*^{KO} background (**Figure 5H**). IgG1^{+} memory B cells were significantly increased in *Tnfaip3*$^{CD11c\text{-}KO}$ compared to *Tnfaip3*$^{CD11c\text{-}HZ}$ mice and *Tnfaip3*$^{CD11c\text{-}WT}$ mice (**Figure 5I**). However, only a minor increase was observed in *Tnfaip3*$^{CD11c\text{-}KO}$*Cd40lg*^{KO} mice (**Figure 5I**).

Taken together, similar to young mice, aged *Tnfaip3*$^{CD11c\text{-}KO}$ mice develop splenomegaly irrespective of the presence of CD40L, with a disturbed splenic architecture. In aged *Tnfaip3*$^{CD11c\text{-}KO}$*Cd40lg*^{KO} mice, GC B cell clusters were absent.

Aged *Tnfaip3*$^{CD11c\text{-}KO}$*Cd40lg*^{KO} mice have IgM and IgA but not IgG1 autoantibodies.

Next, we used flow cytometry to asses IgM^{+}, IgG1^{+} and IgA^{+} plasma cells in the spleens of the six groups of mice. On the *Cd40lg*^{WT} background the proportions of plasma cells that were IgM^{+} were reduced in *Tnfaip3*$^{CD11c\text{-}KO}$ mice, which showed an increase in isotype switched plasma cells, in particular IgG1^{+} (**Figure 6A**). In contrast, the splenic plasma cells in all three *Tnfaip3* genotypes on the *Cd40lg*^{KO} background were mainly IgM^{+}. The remaining (~10%) immunoglobulin positive plasma cells, likely IgG2b, IgG2c or IgG3-positive plasma cells that can occur independently of T-cell interaction[9], did not differ between the genotypes.

Autoreactive anti-dsDNA IgG1 and IgA, but not IgM, were increased in the serum of *Tnfaip3*$^{CD11c\text{-}KO}$ mice compared to WT and *Tnfaip3*$^{CD11c\text{-}HZ}$ controls (**Figure 6B**), as previously shown[4]. Anti-dsDNA IgM was increased in *Tnfaip3*$^{CD11c\text{-}KO}$*Cd40lg*^{KO} mice, compared with *Cd40lg*^{KO} and *Tnfaip3*$^{CD11c\text{-}HZ}$*Cd40lg*^{KO} mice (**Figure 6B**). The absence of CD40L abrogated anti-dsDNA IgG1 and reduced the levels of anti-dsDNA IgA in the serum of the three *Tnfaip3* genotypes. Interestingly however, anti-dsDNA IgA in *Tnfaip3*$^{CD11c\text{-}KO}$*Cd40lg*^{KO} mice was enhanced compared to *Cd40lg*^{KO} mice (**Figure 6B**). Total IgM levels in serum were increased in *Tnfaip3*$^{CD11c\text{-}HZ}$ mice (**Figure 6C**). On *Cd40lg*^{KO} background serum IgM was elevated in both *Tnfaip3*$^{CD11c\text{-}HZ}$*Cd40lg*^{KO} and *Tnfaip3*$^{CD11c\text{-}KO}$*Cd40lg*^{KO} mice (**Figure 6C**). Serum total IgG1 and IgA was elevated in *Tnfaip3*$^{CD11c\text{-}KO}$ mice compared to WT mice and *Tnfaip3*$^{CD11c\text{-}HZ}$ mice, but was significantly lower in *Tnfaip3*$^{CD11c\text{-}KO}$*Cd40lg*^{KO} mice (**Figure 6C**).

Bone marrow (BM) of 24-week-old mice displayed non-significant increases in IgG1^{+} and IgA^{+} memory B-cells in *Tnfaip3*$^{CD11c\text{-}KO}$ mice, which were reduced in *Tnfaip3*$^{CD11c\text{-}KO}$*Cd40lg*^{KO} mice (**Supplementary Figure 4A**). In contrast to spleen, BM plasma cells were reduced in *Tnfaip3*$^{CD11c\text{-}KO}$*Cd40lg*^{KO} mice compared to *Tnfaip3*$^{CD11c\text{-}KO}$ mice (**Supplementary Figure 4B**). The proportions of IgM^{+} plasma cells in BM was lowest in *Tnfaip3*$^{CD11c\text{-}KO}$ mice and *Tnfaip3*$^{CD11c\text{-}KO}$*Cd40lg*^{KO} mice compared to the other four genotypes (**Supplementary Figure 4C**). The high proportions of bone marrow IgG1^{+} and IgA^{+} plasma cells were similar to the results seen in *Tnfaip3*$^{CD11c\text{-}KO}$ mice spleens, with

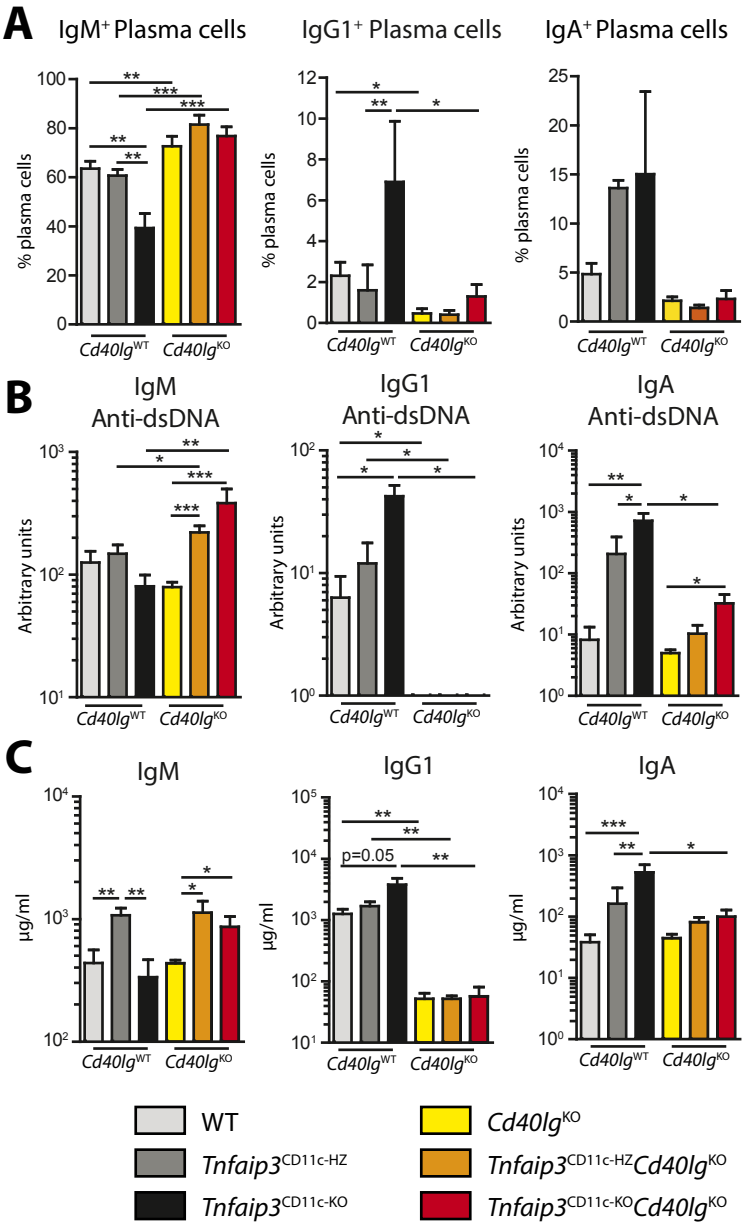

Figure 6: Aged *Tnfaip3*$^{CD11c\text{-}KO}$*Cd40lg*^{KO} mice have IgM and IgA but not IgG1 auto-antibodies.
Naïve 24-week-old *Tnfaip3*^{CD11c}*Cd40lg* mice serum were analyzed. (**A**) Quantification of IgM$^+$ plasma cells (B220$^-$CD138$^+$IgM$^+$), IgG1$^+$ plasma cells (B220$^-$CD138$^+$IgG1$^+$) and IgA$^+$ plasma cells (B220$^-$CD138$^+$IgA$^+$) using flow cytometry. (**B**) Quantification of serum autoreactive IgM, IgG1 and IgA immunoglobulins against ds-DNA using ELISA. **(C)** Quantification of total serum IgM, IgG1 and total IgA using ELISA. Results are pooled from 2-5 independent experiments and are presented as mean values ± SEM of *n* = 11-16 mice per group. *P<0.05, **P<0.01, ***P<0.001, ****P<0.0001. Scale bars represent 200µm.

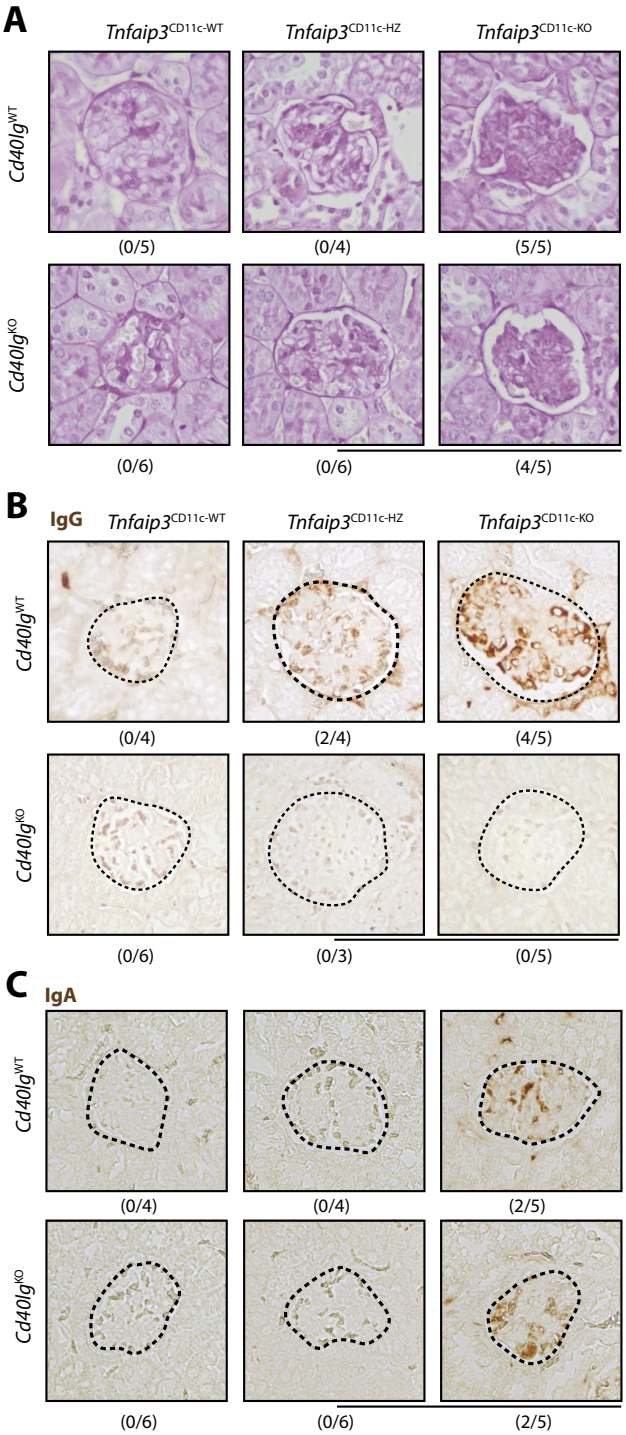

Figure 7: Basement membrane thickening and IgA deposition in kidneys of *Tnfaip3*$^{CD11c\text{-}KO}$*Cd40lg*^{KO} mice. Naïve 24-week-old *Tnfaip3*^{CD11c}*Cd40lg* mice kidneys were analyzed. (**A**) Kidney paraffin slides were stained using Periodic Acid Schiff (PAS)$^{+}$ staining (or PAS-diastase staining). (**B**) Kidney paraffin slides were stained for IgG-positivity using immunohistochemistry. (**C**) Kidney paraffin slides were stained for IgA-positivity using immunohistochemistry. Results are from 4 independent experiments. Scale bars represent 200µm.

drastic reductions of these plasma cells on an *CD40lg*^{KO} background (**Supplementary Figure 4D/E**). A relatively large population of non-IgM/IgG1/IgA plasma cells was seen in *Tnfaip3*$^{CD11c\text{-}KO}$*Cd40lg*^{KO} mice (**Figure 4F**), likely expressing IgG2b, IgG2c or IgG3, given their CD40L-independence[9].

In short, the absence of CD40L hampered the formation of IgG1^{+} plasma cells, leading to a lack of total IgG1 and autoreactive IgG1 in the serum of *Tnfaip3*$^{CD11c\text{-}KO}$*Cd40lg*^{KO} mice. Interestingly, in these mice anti-dsDNA IgM was higher than in the *Tnfaip3*$^{CD11c\text{-}KO}$*Cd40lg*^{WT} counterparts and anti-dsDNA IgA remained detectable.

Basement membrane thickening and IgA deposition in kidneys of *Tnfaip3*$^{CD11c\text{-}KO}$*Cd40lg*^{KO} mice.

Aged *Tnfaip3*$^{CD11c\text{-}KO}$ mice developed inflammatory infiltrates in livers and pancreas islets of Langerhans, which were still present in *Tnfaip3*$^{CD11c\text{-}KO}$*Cd40lg*^{KO} mice but absent in control mice (**Supplementary Figure 5A/B**). As previously demonstrated[4], aged *Tnfaip3*$^{CD11c\text{-}KO}$ mice developed membranoproliferative glomerulonephritis with increased glomerular cellularity and thickening of the basement membranes, compared with *Tnfaip3*$^{CD11c\text{-}HZ}$ mice and WT mice (**Figure 7A**). Interestingly, basement membrane thickening was also observed in kidneys of *Tnfaip3*$^{CD11c\text{-}KO}$*Cd40lg*^{KO} mice, but not in *Cd40lg*^{KO} controls (**Figure 7A**).

Basement membrane thickening in kidneys in lupus glomerulonephritis patients develops due to immunoglobulin complex deposition[27]. Indeed, confirming previous results[4], kidneys of *Tnfaip3*$^{CD11c\text{-}KO}$ mice showed IgG deposition in the glomeruli (**Figure 7B**). However, IgG staining was completely absent in kidneys from all three *Tnfaip3*^{CD11c} genotypes on a *Cd40lg*^{KO} background (**Figure 7B**). Interestingly however, positive glomerular IgA staining could be observed in 2 out of 5 *Tnfaip3*$^{CD11c\text{-}KO}$ mice and *Tnfaip3*$^{CD11c\text{-}KO}$*Cd40lg*^{KO} mice, but was completely absent in the other genotypes (**Figure 7C**).

In summary, basement membrane thickening in *Tnfaip3*$^{CD11c\text{-}KO}$ mice occurs in the absence of CD40L-derived signals and is independent of glomerular IgG deposition. Since IgA deposits were observed in the kidney glomeruli of *Tnfaip3*$^{CD11c\text{-}KO}$*Cd40lg*^{KO} mice, these may well be involved in the induction of basement membrane thickening in the kidneys.

DISCUSSION

DCs critically control immune homeostasis[1]. Mice harboring activated DCs, through ablation of *Tnfaip3*/A20 develop autoimmunity, with increased T cell and B cell activation[3, 4]. *In vitro* B cells could be activated by *Tnfaip3*-deficient BM-DCs without T cell help[4]. In this study, we abrogated T-B cell communication through ablation of CD40L

to examine whether B cell activation could be provoked by *Tnfaip3*-deficient DCs *in vivo* without T cell help[8]. While IgG1 was drastically reduced in *Tnfaip3*$^{CD11c\text{-}KO}$ mice lacking CD40L-signaling, they still developed kidney pathology and (autoreactive) IgA and IgM. T-B cell communication appears therefore not necessary for autoimmune organ inflammation in *Tnfaip3*$^{CD11c\text{-}KO}$ mice.

Using an unbiased approach, we first confirmed by GSEA[17] that full or heterozygote loss of *Tnfaip3* in BM-DCs caused activation, shown by the enrichment for several cytokine-signaling pathways, most prominently "TNF-α signaling via NF-κB". The *in vitro* B cell response driven by *Tnfaip3*-deficient BM-DCs was facilitated by high IL-6 production[4]. *Tnfaip3*-deficient BM-DCs harbored an increased expression of prominent T cell differentiating cytokines, such as IL-12 and IL-23[28] as well as several TI cytokines, such as IL-6[29] and IL-1β[30]. It is puzzling that in our analyses the TI hallmark genes BAFF and APRIL[11] were not significantly upregulated in *Tnfaip3*$^{CD11c\text{-}KO}$ BM-DCs, in contrast to previous publication[4]. In any case, these proteins were not involved in the *in vitro* B cell immunoglobulin production induced by *Tnfaip3*-deficient BM-DCs[4].

As expected, *Tnfaip3*-deficient DCs in spleens of mice harbored an activated phenotype, shown by elevated CD40, CD86 and PD-L1 expression, which appeared to be further elevated when CD40L was absent. Most likely this is not a direct consequence of CD40L-CD40 interaction on DCs, as CD40 signaling in DCs is known to promote the expression of CD80/CD86[31]. It is conceivable that other signals, such as proinflammatory cytokines, promote the increased activation status of DCs.

GC formation critically depends on CD40L-CD40 interaction[32], which we confirmed in both young and aged *Cd40lg*^{KO} mice, as the number of both GC B cells and Tfh-cells were strongly decreased. Despite the absence of clusters of GC B cells and Tfh-cells in *Tnfaip3*$^{CD11c\text{-}KO}$*Cd40lg*^{KO} mice, some B cells could still acquire a GL7^{+} GC B-cell phenotype. During TI immunizations, also in T cell-deficient mice, short-lived GC B cell responses can be induced[33, 34]. As we could not detect clusters of GC B cells in the spleens of *Tnfaip3*$^{CD11c\text{-}KO}$*Cd40lg*^{KO} mice, the GL7^{+} B cell phenotype might be induced by sporadic interaction of B cells and *Tnfaip3*-deficient DCs, promoting their TI activation. In particular MZ B cells are specialized in TI responses[35]. Strikingly, MZ B cells were almost absent in *Tnfaip3*$^{CD11c\text{-}KO}$ mice, but their proportions increased in *Tnfaip3*$^{CD11c\text{-}KO}$*Cd40lg*^{KO} mice. These MZ B cells displayed an activated phenotype, and in contrast to FO B cells, receptors for IL-21 and IL-4 were detected[36, 37]. Elevated expression of IL-4 and IL-21 was seen in CD4^{+} T cells of *Tnfaip3*$^{CD11c\text{-}KO}$*Cd40lg*^{KO} mice. Therefore, these cytokine signals can still be provided by T cells, thereby supporting activation of B cells, in particular of MZ B cells that express receptors for these cytokines.

Unexpectedly, in the absence of appropriate T-B cell communication, *Tnfaip3*$^{CD11c\text{-}KO}$ mice developed glomerulonephritis with glomerular basement membrane thickening. Anti-dsDNA IgG is well-known to cause kidney pathology by depositing in glomeruli

and forming immune complexes[38]. Indeed, IgG was present in kidneys of *Tnfaip3*$^{CD11c\text{-}KO}$ mice, but completely absent in the three *Tnfaip3* genotypes lacking CD40L. Instead, IgA was detected in the glomeruli of a fraction of *Tnfaip3*$^{CD11c\text{-}KO}$*Cd40lg*^{KO} mice, possibly contributing to glomerular membrane thickening, as indeed two out of five mice with IgA deposition had simultaneous glomerular membrane thickening present. Further research is required to identify the mechanisms involved in the kidney pathology in *Tnfaip3*$^{CD11c\text{-}KO}$*Cd40lg*^{KO} mice, particularly in mice that lack IgA complex deposition in the glomeruli. In this context, some SLE patients with glomerulonephritis have high anti-dsDNA IgA titers present[39], which may support the involvement of IgA in kidney pathology. IgA class switch can be induced by IL-6[40] and TGF-β[41]. As IL-6 expression was increased, but TGF-β mRNA expression was low in *Tnfaip3*-deficient BM-DCs (**Figure 1** and previously demonstrated[4, 14] it is conceivable that DC-derived IL-6 may play a prominent role in the induction of heavy chain class switch to IgA in our model. In support of this, in B cell cultures that were stimulated by *Tnfaip3*-deficient BM-DCs neutralization of IL-6 reduced IgA production by ~50%, indicating an important role for IL-6 in mediating increased Ig production when A20 is lacking in DCs. Nevertheless, IL-6 can be produced by a variety of cells, including splenic CD4$^+$ T cells, CD8$^+$ T cells and B cells in *Tnfaip3*$^{CD11c\text{-}KO}$ and *Tnfaip3*$^{CD11c\text{-}KO}$*Cd40lg*^{KO} mice. Therefore, the role of IL-6 in the pathology observed in *Tnfaip3*$^{CD11c\text{-}KO}$*Cd40lg*^{KO} mice is an interesting topic of research in the future. IL-6 is already well recognized as a promising therapeutic target to treat autoimmune diseases[42, 43]. In addition, the increased production of IFN-γ and IL-17 by CD4$^+$ T cells present in *Tnfaip3*$^{CD11c\text{-}KO}$*Cd40lg*^{KO} mice, compared with *Cd40lg*^{KO} mice, may contribute to the autoimmune pathology. Apart from IgA, anti-dsDNA IgM was enhanced in *Tnfaip3*$^{CD11c\text{-}KO}$*Cd40lg*^{KO} mice. We also found total IgM depositions in the glomeruli of these mice, and not in *Tnfaip3*$^{CD11c\text{-}KO}$ mice (data not shown). It is unlikely that these are pathologic immunoglobulin depositions, since autoreactive IgM anti-dsDNA is shown to delay glomerulonephritis in lupus mice[44].

In conclusion, T-B cell communication via CD40-CD40L interaction is not critical for B cell activation, Ig heavy chain class-switch, and autoimmune pathology including glomerulonephritis - possibly mediated by autoreactive IgA - in *Tnfaip3*$^{CD11c\text{-}KO}$ mice. In the context of therapies targeting CD40 or CD40L in human autoimmune diseases[45], it is of relevance that glomerular nephritis can develop independently of IgG deposition and CD40L in mice. However, whether this mechanism also occurs in humans and whether this would involve IgA auto-antibodies remains unknown.

Acknowledgements

We would like to thank Odilia Corneth and the Erasmus MC Animal Facility (EDC) staff for their assistance during the project. This project was supported by The Dutch Arthritis

Association (12-2-410) and the European Framework program 7 (FP7-MC-CIG grant 304221).

Conflict of interest

The authors declare no conflict of interest.

REFERENCES

1. Steinman RM. Decisions about dendritic cells: past, present, and future. *Annu Rev Immunol* 2012; 30: 1-22.
2. Sozzani S, Del Prete A, Bosisio D. Dendritic cell recruitment and activation in autoimmunity. *J Autoimmun* 2017; 85: 126-140.
3. Hammer GE, Turer EE, Taylor KE, Fang CJ, Advincula R, Oshima S *et al.* Expression of A20 by dendritic cells preserves immune homeostasis and prevents colitis and spondyloarthritis. *Nat Immunol* 2011; 12(12): 1184-1193.
4. Kool M, van Loo G, Waelput W, De Prijck S, Muskens F, Sze M *et al.* The ubiquitin-editing protein A20 prevents dendritic cell activation, recognition of apoptotic cells, and systemic autoimmunity. *Immunity* 2011; 35(1): 82-96.
5. Pan L, Lu MP, Wang JH, Xu M, Yang SR. Immunological pathogenesis and treatment of systemic lupus erythematosus. *World J Pediatr* 2019.
6. Malkiel S, Barlev AN, Atisha-Fregoso Y, Suurmond J, Diamond B. Plasma Cell Differentiation Pathways in Systemic Lupus Erythematosus. *Front Immunol* 2018; 9: 427.
7. Fagarasan S, Honjo T. T-Independent immune response: new aspects of B cell biology. *Science* 2000; 290(5489): 89-92.
8. Han S, Hathcock K, Zheng B, Kepler TB, Hodes R, Kelsoe G. Cellular interaction in germinal centers. Roles of CD40 ligand and B7-2 in established germinal centers. *J Immunol* 1995; 155(2): 556-567.
9. Whitmire JK, Slifka MK, Grewal IS, Flavell RA, Ahmed R. CD40 ligand-deficient mice generate a normal primary cytotoxic T-lymphocyte response but a defective humoral response to a viral infection. *J Virol* 1996; 70(12): 8375-8381.
10. Xu J, Foy TM, Laman JD, Elliott EA, Dunn JJ, Waldschmidt TJ *et al.* Mice deficient for the CD40 ligand. *Immunity* 1994; 1(5): 423-431.
11. Xu W, Banchereau J. The antigen presenting cells instruct plasma cell differentiation. *Front Immunol* 2014; 4: 504.
12. Renshaw BR, Fanslow WC, 3rd, Armitage RJ, Campbell KA, Liggitt D, Wright B *et al.* Humoral immune responses in CD40 ligand-deficient mice. *J Exp Med* 1994; 180(5): 1889-1900.
13. van Rijt LS, Prins JB, Leenen PJ, Thielemans K, de Vries VC, Hoogsteden HC *et al.* Allergen-induced accumulation of airway dendritic cells is supported by an increase in CD31(hi)Ly-6C(neg) bone marrow precursors in a mouse model of asthma. *Blood* 2002; 100(10): 3663-3671.
14. Vroman H, Bergen IM, van Hulst JAC, van Nimwegen M, van Uden D, Schuijs MJ *et al.* TNF-alpha-induced protein 3 levels in lung dendritic cells instruct TH2 or TH17 cell differentiation in eosinophilic or neutrophilic asthma. *J Allergy Clin Immunol* 2018; 141(5): 1620-1633 e1612.
15. Trapnell C, Williams BA, Pertea G, Mortazavi A, Kwan G, van Baren MJ *et al.* Transcript assembly and quantification by RNA-Seq reveals unannotated transcripts and isoform switching during cell differentiation. *Nat Biotechnol* 2010; 28(5): 511-515.
16. Trapnell C, Hendrickson DG, Sauvageau M, Goff L, Rinn JL, Pachter L. Differential analysis of gene regulation at transcript resolution with RNA-seq. *Nat Biotechnol* 2013; 31(1): 46-53.
17. Subramanian A, Tamayo P, Mootha VK, Mukherjee S, Ebert BL, Gillette MA *et al.* Gene set enrichment analysis: a knowledge-based approach for interpreting genome-wide expression profiles. *Proc Natl Acad Sci U S A* 2005; 102(43): 15545-15550.
18. Vroman H, Bergen IM, Li BW, van Hulst JA, Lukkes M, van Uden D *et al.* Development of eosinophilic inflammation is independent of B-T cell interaction in a chronic

house dust mite-driven asthma model. *Clin Exp Allergy* 2017; 47(4): 551-564.

19. Das T, Bergen IM, Koudstaal T, van Hulst JAC, van Loo G, Boonstra A *et al.* DNGR1-mediated deletion of A20/Tnfaip3 in dendritic cells alters T and B-cell homeostasis and promotes autoimmune liver pathology. *J Autoimmun* 2019; 102: 167-178.
20. Hunter CA, Jones SA. IL-6 as a keystone cytokine in health and disease. *Nat Immunol* 2015; 16(5): 448-457.
21. Ritvo PG, Klatzmann D. Interleukin-1 in the Response of Follicular Helper and Follicular Regulatory T Cells. *Front Immunol* 2019; 10: 250.
22. Corneth OB, de Bruijn MJ, Rip J, Asmawidjaja PS, Kil LP, Hendriks RW. Enhanced Expression of Bruton's Tyrosine Kinase in B Cells Drives Systemic Autoimmunity by Disrupting T Cell Homeostasis. *J Immunol* 2016; 197(1): 58-67.
23. Vinuesa CG, Linterman MA, Yu D, MacLennan IC. Follicular Helper T Cells. *Annu Rev Immunol* 2016; 34: 335-368.
24. Gonzalez DG, Cote CM, Patel JR, Smith CB, Zhang Y, Nickerson KM *et al.* Nonredundant Roles of IL-21 and IL-4 in the Phased Initiation of Germinal Center B Cells and Subsequent Self-Renewal Transitions. *J Immunol* 2018; 201(12): 3569-3579.
25. Subbarayal B, Chauhan SK, Di Zazzo A, Dana R. IL-17 Augments B Cell Activation in Ocular Surface Autoimmunity. *J Immunol* 2016; 197(9): 3464-3470.
26. Kopf M, Herren S, Wiles MV, Pepys MB, Kosco-Vilbois MH. Interleukin 6 influences germinal center development and antibody production via a contribution of C3 complement component. *J Exp Med* 1998; 188(10): 1895-1906.
27. Yung S, Yap DY, Chan TM. Recent advances in the understanding of renal inflammation and fibrosis in lupus nephritis. *F1000Res* 2017; 6: 874.
28. Zhu J, Yamane H, Paul WE. Differentiation of effector CD4 T cell populations (*). *Annu Rev Immunol* 2010; 28: 445-489.
29. Hirano T, Taga T, Nakano N, Yasukawa K, Kashiwamura S, Shimizu K *et al.* Purification to homogeneity and characterization of human B-cell differentiation factor (BCDF or BSFp-2). *Proc Natl Acad Sci U S A* 1985; 82(16): 5490-5494.
30. Nakae S, Asano M, Horai R, Iwakura Y. Interleukin-1 beta, but not interleukin-1 alpha, is required for T-cell-dependent antibody production. *Immunology* 2001; 104(4): 402-409.
31. Caux C, Massacrier C, Vanbervliet B, Dubois B, Van Kooten C, Durand I *et al.* Activation of human dendritic cells through CD40 cross-linking. *J Exp Med* 1994; 180(4): 1263-1272.
32. Kawabe T, Naka T, Yoshida K, Tanaka T, Fujiwara H, Suematsu S *et al.* The immune responses in CD40-deficient mice: impaired immunoglobulin class switching and germinal center formation. *Immunity* 1994; 1(3): 167-178.
33. Dianda L, Gulbranson-Judge A, Pao W, Hayday AC, MacLennan IC, Owen MJ. Germinal center formation in mice lacking alpha beta T cells. *European journal of immunology* 1996; 26(7): 1603-1607.
34. Lentz VM, Manser T. Cutting edge: germinal centers can be induced in the absence of T cells. *J Immunol* 2001; 167(1): 15-20.
35. Cerutti A, Cols M, Puga I. Marginal zone B cells: virtues of innate-like antibody-producing lymphocytes. *Nat Rev Immunol* 2013; 13(2): 118-132.
36. Turqueti-Neves A, Otte M, Prazeres da Costa O, Hopken UE, Lipp M, Buch T *et al.* B-cell-intrinsic STAT6 signaling controls germinal center formation. *European journal of immunology* 2014; 44(7): 2130-2138.
37. Zotos D, Coquet JM, Zhang Y, Light A, D'Costa K, Kallies A *et al.* IL-21 regulates germinal center B cell differentiation and proliferation through a B cell-intrinsic

mechanism. *J Exp Med* 2010; 207(2): 365-378.

38. Madaio MP, Carlson J, Cataldo J, Ucci A, Migliorini P, Pankewycz O. Murine monoclonal anti-DNA antibodies bind directly to glomerular antigens and form immune deposits. *J Immunol* 1987; 138(9): 2883-2889.
39. Villalta D, Bizzaro N, Bassi N, Zen M, Gatto M, Ghirardello A *et al.* Anti-dsDNA antibody isotypes in systemic lupus erythematosus: IgA in addition to IgG anti-dsDNA help to identify glomerulonephritis and active disease. *PLoS One* 2013; 8(8): e71458.
40. Beagley KW, Eldridge JH, Lee F, Kiyono H, Everson MP, Koopman WJ *et al.* Interleukins and IgA synthesis. Human and murine interleukin 6 induce high rate IgA secretion in IgA-committed B cells. *J Exp Med* 1989; 169(6): 2133-2148.
41. Sonoda E, Matsumoto R, Hitoshi Y, Ishii T, Sugimoto M, Araki S *et al.* Transforming growth factor beta induces IgA production and acts additively with interleukin 5 for IgA production. *J Exp Med* 1989; 170(4): 1415-1420.
42. Ho LJ, Luo SF, Lai JH. Biological effects of interleukin-6: Clinical applications in autoimmune diseases and cancers. *Biochem Pharmacol* 2015; 97(1): 16-26.
43. Wallace DJ, Strand V, Merrill JT, Popa S, Spindler AJ, Eimon A *et al.* Efficacy and safety of an interleukin 6 monoclonal antibody for the treatment of systemic lupus erythematosus: a phase II dose-ranging randomised controlled trial. *Ann Rheum Dis* 2017; 76(3): 534-542.
44. Werwitzke S, Trick D, Kamino K, Matthias T, Kniesch K, Schlegelberger B *et al.* Inhibition of lupus disease by anti-double-stranded DNA antibodies of the IgM isotype in the (NZB x NZW)F1 mouse. *Arthritis Rheum* 2005; 52(11): 3629-3638.
45. Nakamura M, Tanaka Y, Satoh T, Kawai M, Hirakata M, Kaburaki J *et al.* Autoantibody to CD40 ligand in systemic lupus erythematosus: association with thrombocytopenia but not thromboembolism. *Rheumatology (Oxford)* 2006; 45(2): 150-156.

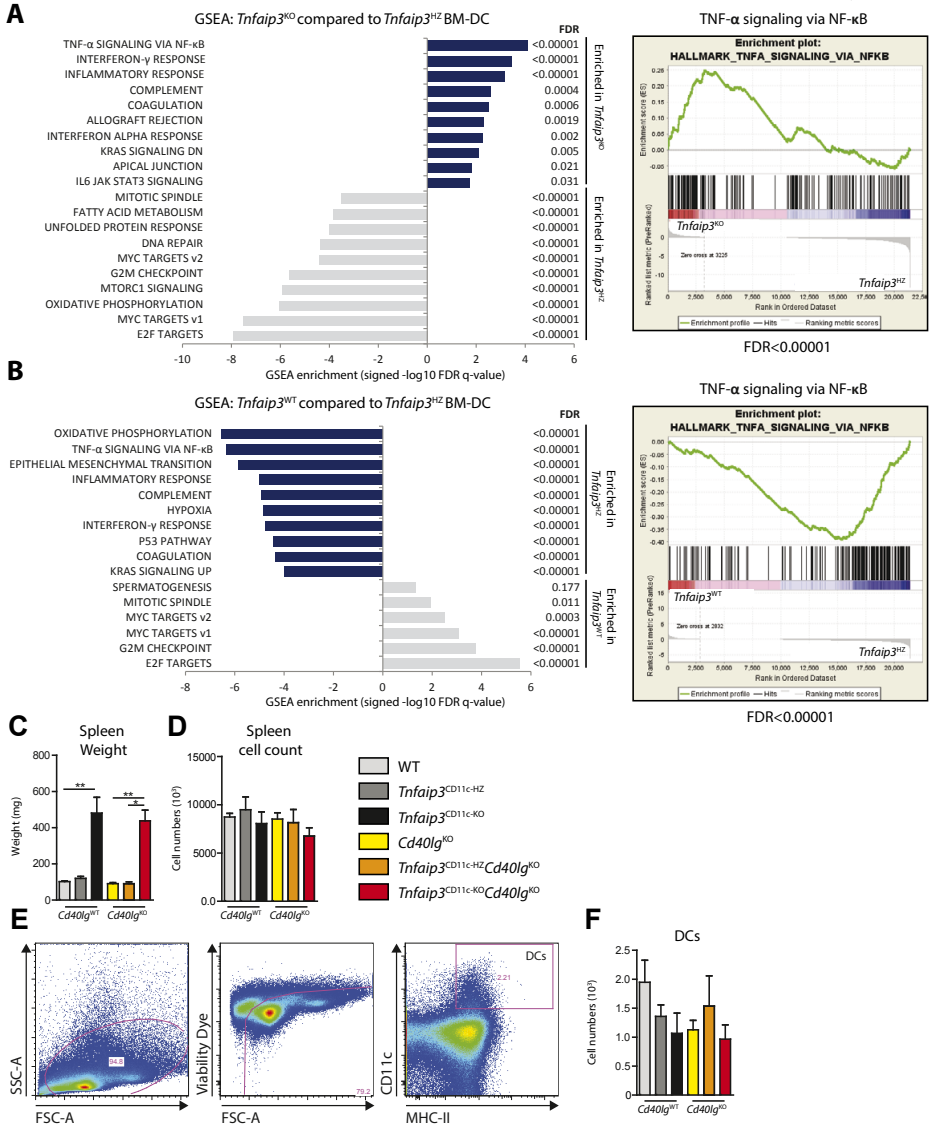

Supplementary Figure 1: BM-DCs and Dendritic cells are activated with loss of Tnfaip3/A20.
BM-derived dendritic cells (BM-DCs) were analyzed by RNA Next generation sequencing (NGS). (**A-B**) Gene set enrichment analysis (GSEA) performed for the ranked list of significantly altered genes between BM-DCs from *Tnfaip3*$^{CD11c\text{-}KO}$ mice and *Tnfaip3*$^{CD11c\text{-}HZ}$ mice (**A**) and *Tnfaip3*$^{CD11c\text{-}WT}$ mice and *Tnfaip3*$^{CD11c\text{-}HZ}$ mice (**B**). Only the top results with a False Discovery Rate (FDR)<0.25 are shown. Enrichments plots for the Hallmark gene set TNFα signaling via NF-κB is also displayed. (**C-F**) Naïve 10-week-old *Tnfaip3*^{CD11c}*Cd40lg* mice spleens were analyzed for (**C-D**) Enumeration of splenic weight (**C**) and cellularity (**D**) using flow cytometry. (**E-F**) Gating strategy for splenic DCs (CD11c^{+}MHC-II^{+}) (**E**) and DC numbers (**F**) using flow cytometry. NGS data is from n=4 BM-DC cultures per genotype. Data in (**C-F**) shown from 2 independent experiments and results are presented as mean values ± SEM of n = 2-7 mice per group. *P<0.05, **P<0.01.

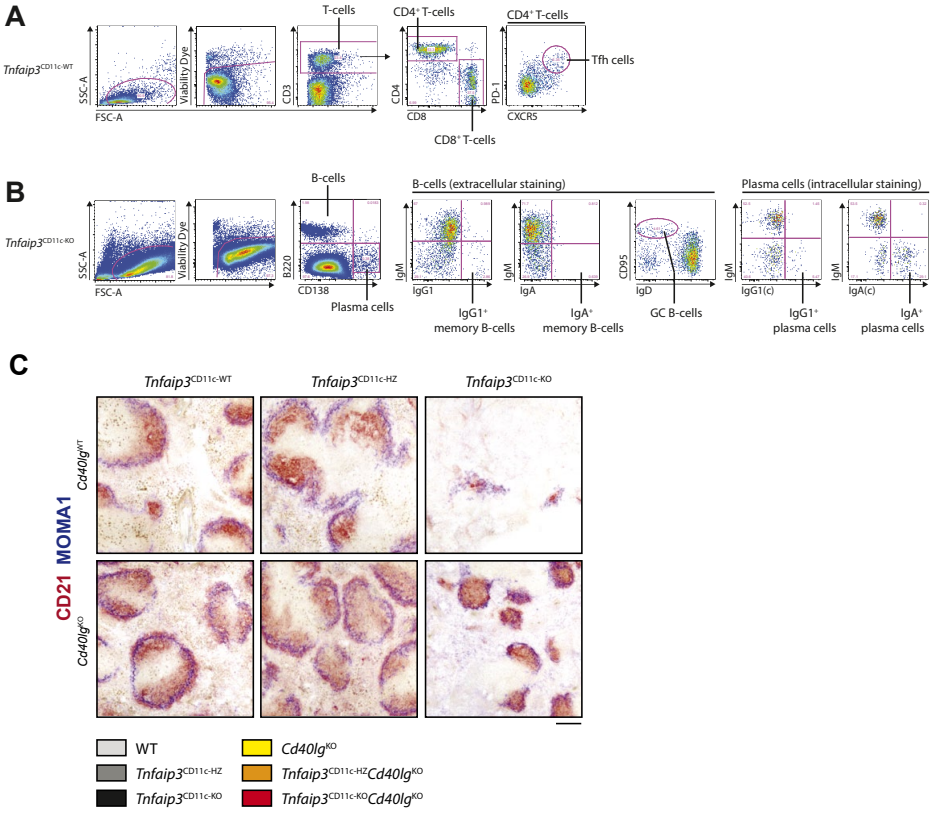

Supplementary Figure 2: Old *Tnfaip3*$^{CD11c\text{-}KO}$ mice have restored MZ B-cells proportions and histology. Gating strategy in naïve *Tnfaip3*^{CD11c}*Cd40lg* spleens to determine T-cells (**A**) and B-cells (**B**) mentioned in Figure 3 and Figure 5. (**C**) Naïve 24-week-old *Tnfaip3*^{CD11c}*Cd40lg* spleens were analyzed by immunohistochemistry. (**C**) Immunohistochemistry of spleens for MOMA1^{+} (Blue) macrophages and CD21^{+} (red) MZ B-cells. Scale bars represent 200µm.

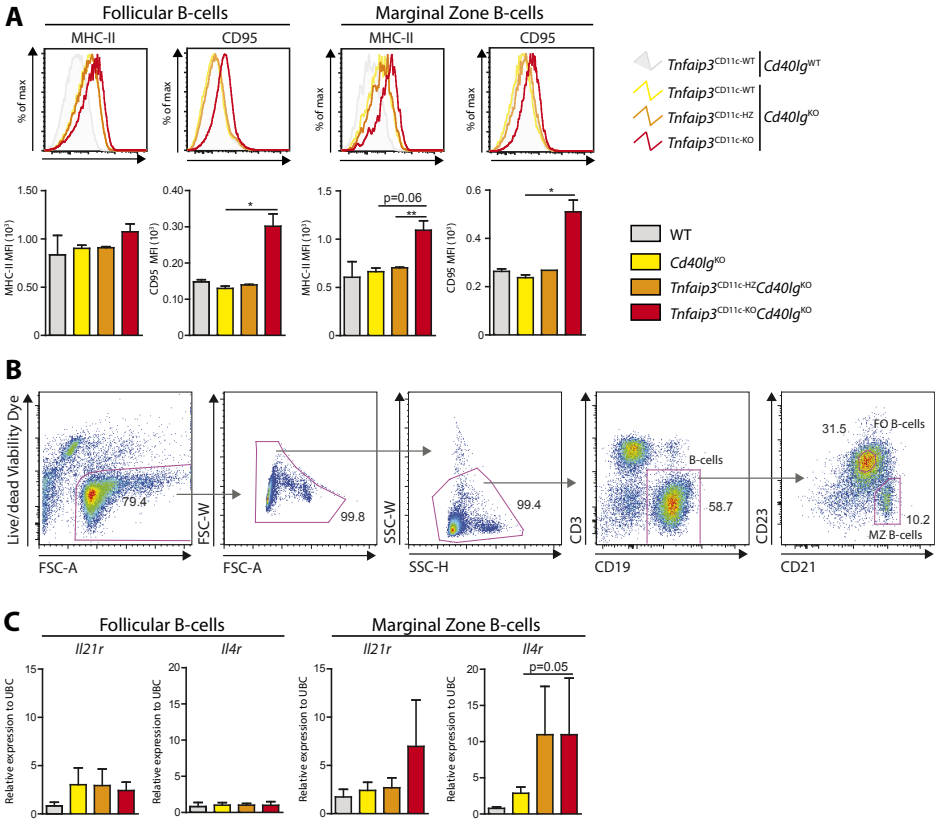

Supplementary Figure 3: Follicular B-cells in Tnfaip3CD11c-KOCd40lgKO mice are also activated, but do not express GC receptors.

Naïve 10-week-old *Tnfaip3*^{CD11c}*Cd40lg* mice spleens were analyzed for FO B-cells (CD19^{+}CD23^{+}, CD21/35^{int}) and MZ B-cells (CD19^{+}CD23^{-}CD21/35^{+}). (**A**) Histograms and barchart quantification of FO B-cell and MZ B-cell MHC-II and CD95 using flow cytometry. (**B**) Flow cytometry sorting gating strategy for both splenic FO B-cells and splenic MZ B-cells. (**C**) Sorted FO B-cells and MZ B-cells from spleens were analyzed using RT-PCR to quantify mRNA levels of Il21r and Il4r. Data is shown from one experiment. Results are presented as mean values ± SEM of n = 2-6 mice per group. *P<0.05, **P<0.01.

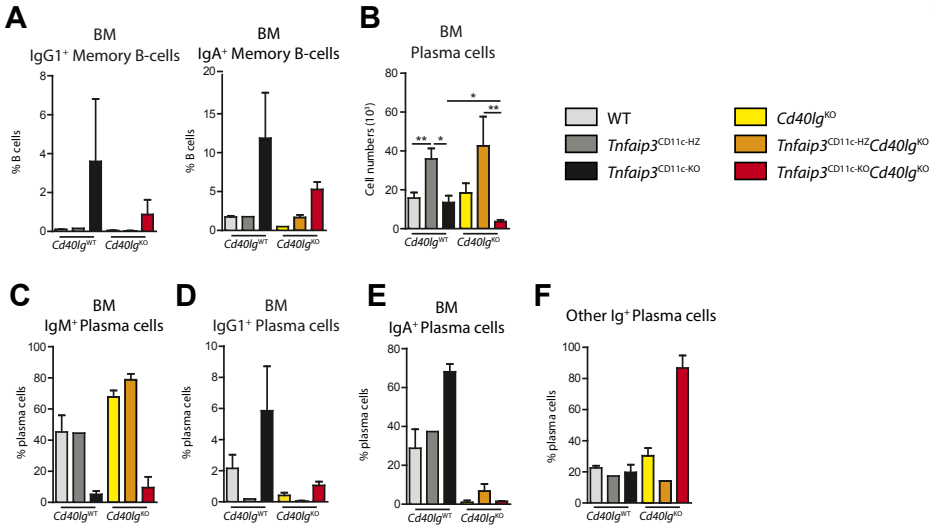

Supplementary Figure 4: Bone marrows of *Tnfaip3*$^{CD11c\text{-}KO}$ mice have enhanced IgG1 B-cells, but not without CD40L signaling.

Analysis of Naïve 24-week-old *Tnfaip3*^{CD11c}*Cd40lg* mice serum and bone marrows. (**A-F**) Enumeration of proportions of IgG1$^+$ Memory B-cells (B220$^+$CD138$^-$IgG1$^+$) and IgA$^+$ memory B-cells (B220$^+$CD138$^-$IgA$^+$) (**A**), plasma cell (numbers B220$^+$CD138$^+$) (**B**) IgM$^+$ plasma cells (B220$^-$CD138$^+$IgM$^+$) (**C**), IgG1$^+$ plasma cells (B220$^-$CD138$^+$IgG1$^+$) (**D**), IgA$^+$ plasma cells (B220$^-$CD138$^+$IgA$^+$) (**E**) and other immunoglobulin-positive plasma cells (B220$^-$CD138$^+$IgM$^-$IgG1$^-$IgA$^-$) (**F**) using flow cytometry. Data is shown of n = 3 independent experiments (in B) and 1 experiments (in A,C-F) and results are presented as mean values ± SEM of n = 2-9 mice per group. *P<0.05, **<P0.01.

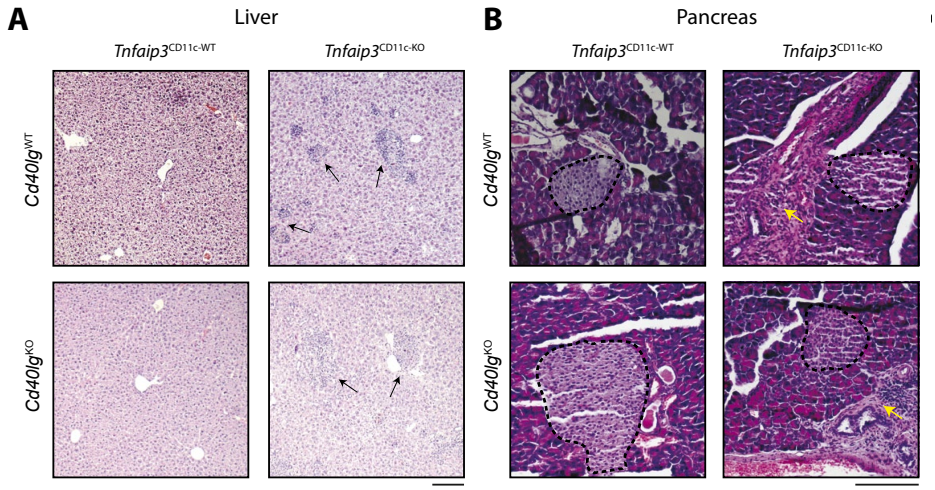

Supplementary Figure 5: Multiorgan inflammation in *Tnfaip3*$^{CD11c\text{-}KO}$ mice occurs independently of T-cell help.

Naïve 24-week-old *Tnfaip3*^{CD11c}*Cd40lg* mice tissues were stained using Hematoxylin and Eosin. Representative Liver (**A**) and Pancreas (**B**) tissues are shown. Liver inflammatory infiltrates (black arrows), islets of Langerhans (Dashed-circle) and Perivascular invlammation (yellow arrows) are depicted. Scale bars represent 200µm.